IEEE Access
Multidisciplinary | Rapid Review | Open Access Journal

Received January 7, 2021, accepted January 20, 2021, date of publication January 25, 2021, date of current version February 5, 2021.

*Digital Object Identifier 10.1109/ACCESS.2021.3054405*

# A Flexible Thermoelectric Generator Worn on the Leg to Harvest Body Heat Energy and to Recognize Motor Activities: A Preliminary Study

**ANTONINO PROTO[1], JAROSLAV VONDRAK[1], MARTIN SCHMIDT[1], JAN KUBICEK[1], OJAN MAJIDZADEH GORJANI[1], JAN HAVLIK[2], AND MAREK PENHAKER[1]**

[1]Department of Cybernetics and Biomedical Engineering, Faculty of Electrical Engineering and Computer Science, VSB-Technical University of Ostrava, 708 00 Ostrava, Czechia

[2]Department of Circuit Theory, Faculty of Electrical Engineering, Czech Technical University, 166 27 Prague, Czechia

Corresponding author: Antonino Proto (antonino.proto@vsb.cz)

This work was supported in part by the European Social Fund (ESF) for International Mobility in the area Biomechanical Energy Harvester for the Recognition of Activities of Daily Living under Grant CZ.02.2.69/0.0/0.0/18_070/0010219, Contract ID: 18_070/0010219-01; in part by the project Biomedical Engineering Systems XVI under Grant SV4500X21.2101, SP2020/55; in part by the Czech Technical University in Prague under Grant SGS20/167/OHK3/3T/13; and in part by the Czech National Library of Technology, CzechELib project.

**ABSTRACT** Wearable devices are commonly used to monitor human movement since motor activity is a fundamental element in all phases of a person's life. Patients with motor disorders need to be monitored for a prolonged period and the battery life can be a limit for such a goal. Here the technique of harvesting energy from body heat to supply energy to wearable devices is investigated. A commercial flexible thermoelectric generator, equipped with an accelerometer, is placed on the lower leg above the ankle. The accelerometer serves to detect diverse motor activities carried out by ten students of VSB-Technical University of Ostrava involved in the execution of two tasks. To summarize, the motor activities analyzed in the proposed work are: ''Sit'', ''Walk'', ''Rest'', ''Go biking'', ''Rest after biking'', and ''Go down and up the stairs''. The maximum measured value of power density was 20.3 $\mu$W cm$^{-2}$ for the ''Walk'' activity, corresponding to a gradient of temperature between the hot and cold side of the thermocouples constituting the flexible thermoelectric generator of 1.5 °C, while the minimum measured value of power density was 8.3 $\mu$W cm$^{-2}$ for the ''Sit'' activity, corresponding to a gradient of temperature of 1.1 °C. Moreover, a mathematical model was developed for the recognition of motor activities carried out during the execution of the experiments. As a preliminary result, it is possible to state that semi-stationary parts of the signal generated by the thermoelectric generator can be traced back to the performance of an activity.

**INDEX TERMS** Body heat, energy harvesting, flexible thermoelectric generator, LTC® 3108, portable data acquisition unit, recognition of motor activities, skin temperature, Tegway Co. Ltd, wearable device.

## I. INTRODUCTION

Since the beginning of the 2000s, wearables have been considered reliable tools for recording data on the health status of human beings [1], [2]. Wearables can be used to monitor the movement of patients with motor disorders, typical of various diseases such as Parkinson's Disease (PD), Spinal Muscular Atrophy (SMA), Cerebral Palsy (CP), among others [3]–[5]. In a rehabilitation process, the record and analysis of data related to kinematic parameters is a useful methodology to understand the effectiveness of a care treatment. However, in the scientific community, physicians and researchers are discussing data discrepancy of a patient's motor skills measured while users are performing tests in medical laboratories compared to when they are performing common daily activities at home. Laboratory measurements are carried out in an artificial environment and last for few minutes; conversely, while performing daily activities, the patient makes more diverse tasks than those performed in a laboratory, so data measured by a physician may be inaccurate and may not properly reflect the patient's real health [6]. As result, it would be more useful to measure people's motor skills, ideally for an unlimited period.

The associate editor coordinating the review of this manuscript and approving it for publication was Tao Wang.

The only possible way to measure kinematic parameters in an unstructured environment for an extensive time is to use wearables: they are low-cost, non-invasive, lightweight, and guarantee comfortability. A wearable device can sense physiological data, extract relevant information, and communicate the outcome via a wireless interface [7].

Battery capacity limits the device operating time. Increasing the mass of the active materials in the battery allows a longer device operating time, but its size and weight will increase at the expense of the fit of device. Thus, the challenge for all developers around the world is to provide wearables that work as long as possible or that do not need to be recharged. Indeed, for the continuous monitoring of data related to human movement, there is an absolute need of energy harvesting solutions to extend the operating time of a wearable for many hours or days.

A conceivable way to resolve this issue is to harvest the energy generated by the human body. The potential energy sources of the body include kinetic energy through the movements of body joints and thermal energy in the form of heat exchanged between the body and the environment [8], [9]. The kinetic energy source only exists if the body is in motion, while the thermal energy is always present because the dissipation of body heat is a continuous physical phenomenon. About the literature on human body energy harvesting, the value of power density generated by a thermoelectric harvester is approximately 30 $\mu$W cm$^{-2}$, while the value generated by a kinetic one does not exceed 5 $\mu$W cm$^{-2}$ [10]. Therefore, it seems appropriate to focus the proposed research on techniques for harvesting the body's thermal rather than biomechanical energy.

### A. THERMOELECTRIC GENERATOR

Fig. 1 shows a schematic of a thermal circuit where the load is represented by a ThermoElectric Generator (TEG). The equivalent electrical circuit for the TEG is shown in the red dashed box of Fig. 1. The TEG is the device commonly used to transduce thermal energy into electricity by exploiting the Seebeck effect, for which a voltage difference is generated when a temperature difference appears between the two ends of a material, *e.g.*, metal or semiconductor [11], [12]. A TEG is made up of multiple thermocouples (TCs), which are usually composed by p- and n-type semiconducting leg materials electrically connected in series through metal electrodes, and commonly encapsulated between two ceramic plates [13].

While considering the thermal circuit of Fig. 1, the rate of heat transfer across the TEG, $\dot{Q}$, can be estimated as:

$$\dot{Q} = \frac{\Delta T'}{R_{TEG}} \tag{1}$$

where $\Delta T' = T'_H - T'_C$ is the temperature difference between the hot and cold sides of the TCs, and $R_{TEG}$ is the thermal resistance of the TEG. In the electrical circuit, the TEG is represented by a voltage generator modelled as an ideal voltage source in series with a resistor, which is the internal electrical resistance, R. The value of Seebeck coefficient, $\alpha$, describes

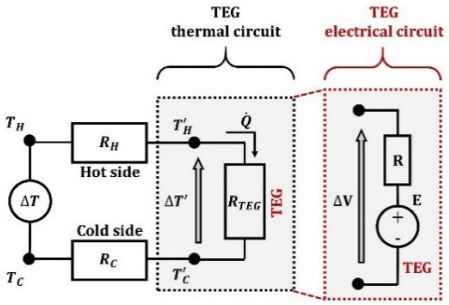


**FIGURE 1. Schematic of a thermal circuit where the TEG is the thermal load. The red dashed box shows the TEG equivalent electrical circuit.**

the voltage difference generated from the temperature difference across the TCs. Since the TCs are made by p- and n-type semiconducting legs, the TEG Seebeck coefficient, $\alpha_{\mathrm{pn}} = (\alpha_{\mathrm{p}} - \alpha_{\mathrm{n}})$, results as it follows:

$$\alpha_{\mathrm{pn}} = -\frac{\Delta \mathrm{V}}{\Delta T'} \tag{2}$$

The thermoelectromotive force of the voltage generator, E, depends on the temperature difference across the TCs of the TEG, $\Delta T'$, on the total number of TCs constituting the TEG, $N$, and on the Seebeck coefficient, $\alpha_{\mathrm{pn}}$, [14]:

$$\mathrm{E} = N\alpha_{\mathrm{pn}}\Delta T' \tag{3}$$

TEGs are used in many applications ranging from medical and wearable devices to many different systems for the industry [14]. About the industry, the current main application for thermal energy harvesting regards the automotive sector. TEGs are placed inside the vehicle to harvest the heat wasted by exhaust gas to improve engine performance and decrease the fuel energy costs [15]; waterproof TEGs can also be implemented in ships or submarines to generate electrical power from the energy densities of hydrothermal fluids in the deep-sea [16]. In addition, TEGs are being used to supply energy to wireless sensor nodes for the application field of the Internet of Things. TEG-based architectures are implemented in sensor networks to solve the issue of prolonged operating time for the continuous transmission of data regarding temperature, humidity, pollution, and surveillance management, among others [17].

There are three main approaches to develop a TEG, which depend on the arrangement of the p- and n-type legs and on the direction of the heat flow through the TEG. These approaches include: (i) lateral heat flow and lateral arrangement, (ii) vertical heat flow and vertical arrangement, and (iii) vertical heat flow and lateral arrangement [14]. About applications on thermal energy harvesting from the heat dissipated by the human body, the main approaches are the second and the third. Using the first approach, the conduction of heat takes places between different parts of the body, and not from the body to the environment [18].

Nowadays for applications concerning body heat energy harvesting, a common rigid TEG is usually replaced by

a flexible-TEG (F-TEG), since the irregular shape of the body does not allow proper contact between the skin and the rigid TEG. Fig. 2 shows the difference between a rigid TEG and an F-TEG, for which the rigid ceramic substrates disappear, and the air gap between the p- and n-type legs is filled by a polymeric matrix, which guarantees flexibility and robustness to the entire structure.

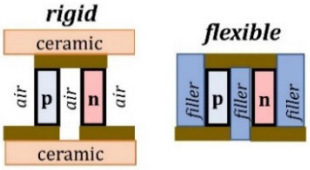


**FIGURE 2.** Cross-sectional views of a rigid and flexible TEG. For simplicity, the TEGs consist of a single TC.

The Carnot cycle defines an upper limit on how the heat dissipated into the environment can be harvested. This limit is defined by the Carnot efficiency, $\eta_c = \frac{T_H - T_C}{T_H}$. Regarding the body heat energy harvesting process, assuming the body temperature, $T_H = 37\,^{\circ}\text{C}$, and air temperature, $T_C = 21\,^{\circ}\text{C}$, the resulting efficiency is approximately 4.3% [19]. However, the maximum conversion efficiency of the TEG can be estimated as a fraction of $\eta_c$, as it follows:

$$\eta_{\max} = \eta_c \frac{\sqrt{1 + ZT_{\text{pn}}} - 1}{\sqrt{1 + ZT_{\text{pn}}} + \frac{T_C}{T_H}} \tag{4}$$

where $ZT_{\text{pn}}$ is the dimensionless figure-of-merit of the p- and n-type TC, and it is defined as [14]:

$$ZT_{\text{pn}} = \frac{\alpha_{\text{pn}}^2}{\left[\left(\rho_{\text{p}}\kappa_{\text{p}}\right)^{0.5} + \left(\rho_{\text{n}}\kappa_{\text{n}}\right)^{0.5}\right]^2} T \tag{5}$$

where $T$ is the absolute temperature of the p- and n-type TC, $\rho$ is the electrical resistivity and $\kappa$ is the thermal conductivity of the p- and n-type legs, respectively. For a TEG module made from a specific number, $N$, of TCs, the whole figure-of-merit is given by [14]:

$$ZT_{\text{TEG}} = \left(N\alpha_{\text{pn}}\right)^2 \frac{R_{TEG}}{\text{R}} T \tag{6}$$

where R is the internal electrical resistance and $R_{TEG}$ the thermal resistance of the TEG.

Many factors affect the performance of a body heat energy harvesting system, such as the physical characteristics of living tissues, physiological state of the body, environmental conditions, as well as thermal and electrical features of the thermoelectric materials employed for developing a TEG [20], [21].

While harvesting the energy from the body heat dissipated in the environment, the amount of voltage generated by the TEG is in the order of millivolts, which is less than the value of the input voltage required by commercial off-the-shelf (COTS) components to operate. Thus, it is mandatory to use a power management circuit to increase the TEG voltage output to a required value, which is in order of magnitude of volts. This will further decrease the efficiency of the energy harvesting process, so that the amount of thermal energy collected on the bodily surfaces might be not enough to power a wearable device continuously.

The challenge of this work concerns the use of a TEG to understand if the body heat energy, harvested while users perform motor activities, is enough to power sensors used in monitoring people's movement for an unlimited period. Moreover, an analysis on the pattern of the TEG output signals is carried out to correlate those signals with the diverse performance of human activities. In such a way, TEGs may be used to distinguish movements performed in common life scenarios. In the scientific literature, there is a lack of studies aimed at using thermoelectric energy harvesters to detect people's motor activities. The proposed work addresses this topic at a preliminary stage.

In the following paragraphs, first the materials chosen for the execution of the tests and the experimental setup will be introduced. Then, the procedure for carrying out the experiment and the techniques used for data processing will be explained. The collected data will be shown in the "Results" section and analyzed in the "Discussion" section. Finally, the "Conclusions" section emphasizes the results of the work.

## II. MATERIALS AND METHODS

To monitor the thermoelectromotive force, *i.e.*, Seebeck voltage, generated while people were moving and to detect diverse human activities, it was necessary to combine an F-TEG, suitable for wearing, and an accelerometer useful for monitoring human motor activities. A data acquisition unit (DAU) was also built for saving all the measured signals. In the aftermath, data were processed offline through the MATLAB® SW environment.

Fig. 3 shows the wearable system used by users during the execution of diverse activities. An F-TEG and an accelerometer were placed on both the legs, above the ankle. Connection wires, of approximately 110 cm, bridge the output signals of the F-TEG and accelerometer to the input pins of the DAU. To reduce discomfort while performing the activities, a support Velcro belt was used to place the DAU at the level of the waist. (see Supplementary Material Video).

### A. HARDWARE

The circuit schematic of the proposed wearable measurement system is shown in Fig. 1S (see Supplementary Material).

#### 1) F-TEG

The fully-flexible thermoelectric device is the F-TEG developed by Tegway Co. Ltd. Company, South Korea. It is the world-first "stand-alone" high performance F-TEG, and it is the output of the research effort conducted by the Korea Advanced Institute of Science and Technology (KAIST). The information related to the manufacturing process and its characterization, can be found in [22]–[24].

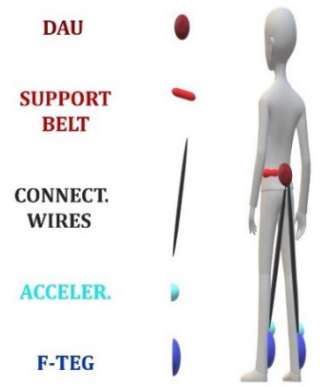


**FIGURE 3.** Wearable system used by users.

The F-TEG module encapsulates 170 couples of p- and n-type legs (p-type: $Bi_{0.3}Sb_{1.7}Te_3$, n-type: $Bi_2Se_{0.3}Te_{2.7}$). The p- and n-type legs are dices with dimensions: 1.6 mm × 1.6 mm × 2.0 mm. Fig. 4 shows the hot side of the F-TEG, which faces the human skin (red dashed box), while the cold side is facing the environment (blue dashed box). The F-TEG is worn above the ankle and the proper contact with the skin is guaranteed by Velcro straps. The F-TEG is equipped with a superabsorbent polymer-based heatsink that promotes liquid evaporation to allow the F-TEG to obtain a larger temperature difference between its two sides, which leads to higher power generation. When combining the use of the heatsink with the F-TEG, the heatsink needs to be wet and squeezed before its placement on the F-TEG. The same F-TEG has already been used to supply energy for performing a wearable electrocardiography [25].

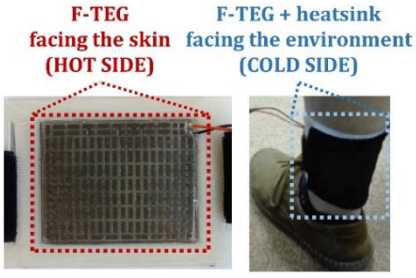


**FIGURE 4.** The F-TEG device, and the F-TEG worn above the ankle.

Compared to a common rigid TEG, the F-TEG eliminates the ceramic substrate plates, while filling the empty space between the p- and n-type legs with a proprietary polymer material, *i.e.* polyurethane filler foam [26]. The adhesive strength between the foam and the p- and n-type legs, as well as between the foam and the copper connections is high enough to make the F-TEG reliable to be used on the curved shapes of the body [26].

While considering the thermal resistance of the F-TEG, $R_{TEG}$, it is modelled by the parallel combination of the thermal resistance of the p- and n-type legs, $R_{le}$, with the thermal resistance of the filler, $R_{fi}$, which can be estimated as [27]:

$$\kappa R_{le} = \frac{h}{2Nw^2}\frac{1}{\kappa_{le}} \tag{7}$$

$$\kappa R_{fi} = \frac{h}{A - 2Nw^2}\frac{1}{\kappa_{fi}} \tag{8}$$

where $A$ is the entire area of the F-TEG, $h$ is the height and $w$ the width of a leg, and $\kappa_{le}$, $\kappa_{fi}$ are the thermal conductivity of the legs and the filler, respectively. The value of $\kappa_{le}$ is the average of p-type, $\kappa_p$, and n-type, $\kappa_n$, thermal conductivity values.

The internal electrical resistance of the F-TEG, R, can be calculated as the sum of the electrical resistances of the p- and n-type legs, and the electrical resistance of the copper contacts that connect each leg of the F-TEG [14]:

$$\mathrm{R} = N\left(\frac{h_p\rho_p}{A_p} + \frac{h_n\rho_n}{A_n} + 2\frac{h_{Cu}\rho_{Cu}}{A_{Cu}}\right) \tag{9}$$

where $h_p = h_n$ are the lengths of each leg crossed by the heat flow, $A_p = A_n$ are the cross-sectional areas of the legs, $h_{Cu}$ is the length and $A_{Cu}$ the cross-sectional area of each contact, and $\rho_p$, $\rho_n$, $\rho_{Cu}$ are the electrical resistivity of the elements.

Fig. 5 shows the electrical circuit for the measurement of the voltage output, $V_L$, across a resistor load, $R_L$. The op-amp serves to amplify the voltage output signal to meet the requirements given by the input voltage range of the analog-to-digital converter of the DAU. The input impedance of the op-amp, $Z_{in} = 50\ k\Omega$, is much larger than $R_L$, so it is negligible for the calculation of $V_L$.

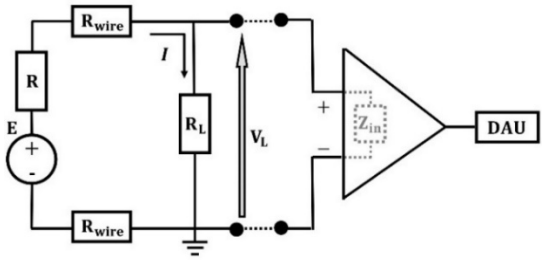


**FIGURE 5.** Electrical circuit for the measurement of the F-TEG voltage output across a resistor load.

While measuring $V_L$, it is important to consider the electrical resistances of the copper connection wires, $R_{wire}$, because the wires are 110 cm long, and their resulting resistance value differs by only an order of magnitude with respect to the value of R, so as $R_{wire}$ can distort the effective measured values, $V_L$, which is given by the following equation:

$$\mathrm{V_L} = \mathrm{E}\frac{\mathrm{R_L}}{(\mathrm{R_L} + \mathrm{R'})} \tag{10}$$

where $R' = R + 2R_{wire}$, (about values for the calculation of thermal and electrical resistances, see Table IS in Supplementary Material).

According to the maximum power transfer theorem, the optimum value for the electrical resistance load,

$R_L$, should match the value of $R'$, ($R_L = R'$), in order to obtain the maximum value of power generated by the F-TEG:

$$P_{L_{MAX}} = \frac{E^2}{4R'} \tag{11}$$

However, since the F-TEG is a non-linear device, the value of $R_L$ is shifted to a larger resistance value, which is usually estimated to be $\sim$1.4 $R'$ [28], but it can also reach the value of $\sim$1.8 $R'$ [29]. For that reason, the formula for the calculation of the power generated by the F-TEG is as follows:

$$P_L = \frac{V_L^2}{R_L} = E^2 \frac{R_L}{(R_L + R')^2} \tag{12}$$

While performing the experiments, a 3.3 Ω resistor load, $R_L$, was connected to the ends of the F-TEG. This value was carefully established in a previous work done by our research group [30]. The device and thermoelectric parameters are summarized in Table 1.

**TABLE 1. F-TEG – device and thermoelectric parameters.**

| Device parameters | Value | Unit |
|---|---|---|
| Dimension | 84.82 × 63.8 × 2.2 | mm |
| p- and n-type pairs | 170 | couples |
| Fill factor | ~ 16 | % |
| Application temperature | < 100 | °C |
| Flexibility (bend. radius) | X axis: < 10<br>Y axis: < 10 | mm |
| **Thermoelectric parameters** | **Value** | **Unit** |
| Electrical conductivity, $\sigma$ | p-type: 2028<br>n-type: 1651 | S cm$^{-1}$ |
| Thermal conductivity, $\kappa$ | p-type: 1.73<br>n-type: 1.88 | W m$^{-1}$ K$^{-1}$ |
| Seebeck coefficient, $\alpha$ | p-type: 176<br>n-type: -161 | μV K$^{-1}$ |
| AC electrical resistance, $R_{AC}$ | *at* 27 °C: 2.95 ± 0.1 | Ω |
| Figure of merit, $ZT_{TEG}$ | ~ 0.72 | --- |

### 2) ACCELEROMETER

The accelerometer chosen for this work is the ADXL362, Analog Devices. It is a micropower, 3-axis, digital output inertial sensor that communicates with the DAU via an SPI interface.

The placement of the accelerometer above the ankle guarantees the calculation of the frequency value of the performed activity. We selected the data in the sagittal plane of the 3D-accelerometer. To obtain frequency-based features, Fast Fourier Transform (FFT) was applied to calculate the resulting frequency value for each activity performed.

About rehabilitation purposes, the inertial sensor mounted on the lower leg returns the most accurate information for estimating spatial and temporal parameters of normal and impaired gaits [31], [32].

### 3) DATA ACQUISITION UNIT – DAU

Acquisition of data was performed by using an Arduino Uno board equipped with an Adafruit data logging shield. The data logging shield serves to enable the saving of the measured data on an SD card via SPI digital communication. A case with 6 AA batteries was attached to the DAU as well, in order to provide power to the Arduino with a voltage of 9 V.

Each leg of the subject was equipped with the F-TEG, the output of which was loaded with a 3.3 Ω resistor. The voltage difference on the load was then amplified by an LM386 low voltage amplifier to meet the requirement given by the range scale of the analog-to-digital converter of the DAU. The internal gain of the amplifier is set by default to 20 and can only be increased by adding an external resistor. For the purpose of this experiment, this default amplification value was used. The output of LM386 is biased to half the supply voltage. The supply voltage from the Arduino was supposed to be 5 V, but when measured with a voltmeter it was closer to 4.36 V. The lower voltage decreases the resolution of the ADC. The ADC on the Arduino input pins is 10-bit, which should provide a resolution of 4.9 mV if the signal ranges from 0 to 5 V. With the gain of 20 used in this circuit, the resulting data will have a resolution of 0.245 mV. This means that the maximal value of the TEG signal before ADC saturation should be 2.5 V divided by a gain of 20. That would be 125 mV. However, with the supply closer to 4.36 V, the maximal value read from the TEG device is about 93 mV. The amplification circuit with LM386 is soldered on the data logging shield.

The device can be started by plugging in the battery power supply. Arduino first initializes the SPI bus, sets the accelerometers for the ±4 g range and then starts the measurement. In each loop of the program, all the measured data were saved as one line of a comma-separated value file created on the SD card. The collected data include the x, y, z axes of both accelerometers, voltages measured from the F-TEGs and time since the start of the measurement. Each start of the device creates a new numbered file on the SD card. The data collection sampling frequency was set to 19 Hz.

### 4) TESTING THE F-TEG AS POWER SOURCE TO SUPPLY ENERGY TO AN ANALOG ACCELEROMETER

To test the performance of F-TEG as a power source, an analog accelerometer was chosen as the sensor to be powered.

An analog sensor has been selected instead of the ADXL362 digital one since the latter must be connected to a microcontroller through a serial interface, in which a voltage passage occurs. Thus, to be sure to get the only voltage source, the voltage given by the F-TEG, the FXLN8361Q analog accelerometer was chosen to perform this experiment. The supply voltage for this sensor is from 1.71 to 3.6 V, with a current consumption of 180 $\mu$A.

The F-TEG voltage output is stepped up through the LTC3108 DC-DC converter, which uses a small transformer to provide a complete power management solution. The FXLN8361Q analog accelerometer is the load of the circuit. The hardware schematic is shown in Fig. 2S (see Supplementary Material).

The voltage output of the LTC3108, $V_{OUT}$, charges a 660 $\mu$F capacitor to 3.3 V. Once the capacitor has been charged to this voltage value, the LTC3108 enables the

charging, to 5V, of an auxiliary 100 $\mu$F capacitor, which is connected between the $V_{STORE}$ pin of the DC-DC converter and the ground. The accelerometer was then manually switched on when both capacitors were fully charged.

### B. THERMAL MEASUREMENTS

Fig. 6 highlights the temperature gradients of the thermal system, which consists of the human body, the F-TEG, and the air. In the same way as Fig. 1, $\Delta T = T_H - T_C$ is the temperature difference between the body and the environment, while $\Delta T' = T'_H - T'_C$ is the temperature difference between the hot and the cold side of the TCs, which form the F-TEG.

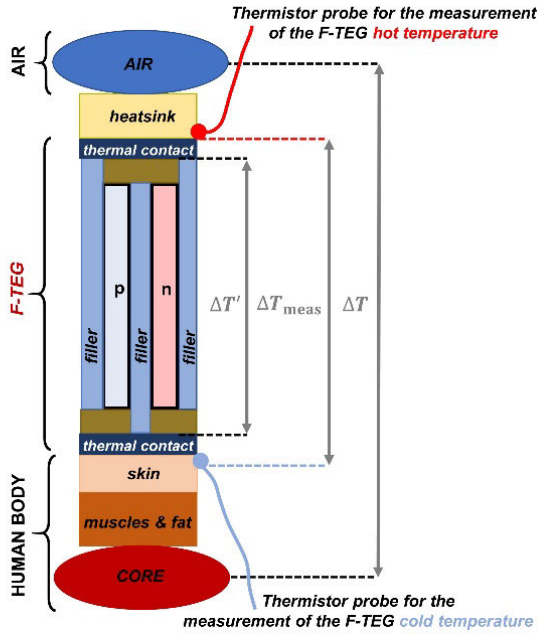


**FIGURE 6.** Temperature gradients of thermal system, and positions where the thermistor probes are placed to measure $\Delta T_{meas}$.

Once the voltage value $V_L$ is measured across the load, the value of $\Delta T'$ is easily calculated through Eqs. (3) and (10). However, there is a difference between the value of $\Delta T'$ and the value of temperature difference across the F-TEG, $\Delta T_{meas}$, which is experimentally measurable with a multichannel recording system composed by integrated thermistor probes that can be directly placed on the hot and cold side of the F-TEG.

To monitor the value of $\Delta T_{meas}$, the temperature of the hot side of the F-TEG is measured by placing a thermistor probe at the interface between the skin and the F-TEG, while the temperature of the cold side is measured with another thermistor probe placed between the F-TEG and the heatsink. The integrated thermistor probes are the NTC 10K3MBD1, having time response of 400 ms and resolution $\pm 0.2$ °C in the temperature range from 0 °C to +70 °C. The temperature measurement system used to monitor the value of $\Delta T_{meas}$ is custom made and it has already been used by our research group in [33]–[35].

Temperature measurements of the skin and the environment were carried out with a SkyRC ITP380 Thermometer; it is equipped with a high-speed infrared sensor: precision of $\pm 0.5$ °C in the temperature range from 0 to 60 °C. Temperature values of both the left and right leg of each participant where the F-TEG is worn were measured at the beginning and the end of the experiment. These measurements serve to verify the decrease of the temperature on the skin due to the direction of the heat transfer from the core to the environment, which takes place perpendicular to the surface of the body.

### C. PROCEDURE AND DATA PROCESSING

Two structured scenarios were investigated in the proposed experiment: (1) a task to be carried out solely into a laboratory environment (*L-task*), and (2) a task to be carried out both in the laboratory, corridor, and stairs of the VSB-Technical University of Ostrava (*LCS-task*). Each task is divided into diverse motor activities, as it follows.

Task in laboratory (*L-task*):

- Activity 1. Begin; to sit.
- Activity 2. Walk slowly.
- Activity 3. Standing: first rest.
- Activity 4. Walk at preferred speed.
- Activity 5. Standing: second rest.
- Activity 6. Walk quickly.
- Activity 7. Standing: third rest.
- Activity 8. Walking to the rhythm of 120 bpm.
- Activity 9. Standing: fourth rest.
- Activity 10. Go biking to the rhythm of 60-bpm.
- Activity 11. On the exercise bike: fifth rest.
- Activity 12. Go biking to the rhythm of 90-bpm.
- Activity 13. On the exercise bike: sixth rest.
- Activity 14. Go biking to the rhythm of 120-bpm.
- Activity 15. On the exercise bike: seventh rest.
- Activity 16. End; to sit.

Task in laboratory, corridor and stairs (*LCS-task*):

- Activity 1. Begin; to sit in laboratory.
- Activity 2. First walk in the corridor.
- Activity 3. Standing in the corridor: first rest.
- Activity 4. Second walk in the corridor.
- Activity 5. Standing in the 3$^{rd}$ floor of the stairs: second rest.
- Activity 6. Going downstairs.
- Activity 7. Standing in the 1$^{st}$ floor of the stairs: third rest.
- Activity 8. Going upstairs.
- Activity 9. Standing in the 3$^{rd}$ floor of the stairs: fourth rest.
- Activity 10. End; to sit in laboratory.

The raw data of the accelerometers and F-TEGs were stored on an SD card as.csv files. The data processing was done offline when users concluded performing the task, whether it was an *L-* or *LCS-task*.

F-TEG output data, *i.e.*, voltage signals $V_L$, were smoothed by a third-order, low-pass, Butterworth filter with a cut-off frequency of 8 Hz.

Then, each signal was manually segmented to differentiate the diverse motor activities; indeed, voltage values are increasing or decreasing over the time based on the activity performed.

In order to recognize the performance of different motor activities, the computing of a mathematical method for the detection of semi-stationary parts of the signal can be useful. The recognition of an activity can be detected if the signal shape does not change excessively over the time. Conversely, if the signal amplitude quickly changes, it will mean that a change from the previous activity has occurred.

The calculation of the signal gradient is a technique to separate the stationary and dynamic parts of a signal. The gradient represents the direction of a slope, and it is a differential operator. The result of the calculated gradient is a vector field, which expresses the direction and magnitude of the highest change of the scalar field.

While analyzing the F-TEG voltage output signal, stationary parts will have an insignificant down to zero gradient level. Conversely, for dynamic parts of the signal, the calculated gradient level will be large. Therefore, it is necessary to set a gradient threshold to determine the aforementioned signal parts. To do it, the global maximum of the gradient, $G_{max}$, is computed. Moreover, the square value of the signal gradient, $G^2$, is calculated because it ensures the emphasis of the information on the highest gradient, as opposed to the low values of the gradient that are suppressed. The formula used to recognize, or not, an activity is as follows:

$$G^2 > xG_{max} \Rightarrow \text{activity not recognized} \quad (13)$$

$$G^2 \leq xG_{max} \Rightarrow \text{recognized activity} \quad (14)$$

where $x$ is the percentage of the gradient maxima to compute the threshold.

## III. RESULTS

Four participants performed the *L-task* (age: 22–25 years, body weight: 52–72 kg, height: 160–176 cm; three females), and six participants performed the *LCS-task* (age: 22–25 years, body weight: 51–88 kg, height: 160–188 cm; five females). All of them are students of VSB-Technical University of Ostrava. They have no motor disorders and before starting the experiment they gave written informed consent for carrying out the experiment.

Based on the physical characteristics of the participants, the body mass index was calculated (BMI; in kg $m^{-2}$); the BMI value indicates if the weight is healthy [36]. Significant subcutaneous fat deposits counteract the core-to-skin heat dissipation, resulting in less energy harvested by the F-TEG [37]. Anyway, participants were in the healthy weight range because all calculated BMI values are between 18.5 and 24.9 (Tables 2S and 3S in Supplementary Material) [38].

Figs. 7 and 8 show the patterns of the power generated by the F-TEG (black line), the accelerometer magnitude (grey line) that indicates the difference between static and dynamic activities and the total energy harvested by the F-TEG (red line). About the accelerometer magnitude signal, the unit of measurement is not displayed because such a signal was only used to distinguish the diverse activities carried out in the experiment, so that to help for the signal segmentation in order to create data groups for comparing the different activities.

The values of power generated by the F-TEG were calculated with Eq. (12) by using the measured voltage signals $V_L$, while values of the energy harvested were computed through cumulative trapezoidal numerical integration, *i.e.* cumtrapz MATLAB® function. Fig. 7 shows the signals related to the right leg of student four, while Fig. 8 to the right leg of student six. The pattern of signals in these figures are like those obtained for all students. In Supplementary Materials, the F-TEG voltage signals of each student are shown in Figs 3S, 4S.

Tables 2 and 3 list the average and standard deviation values of power, $P_L$, and temperature difference across the TCs of the F-TEG, $\Delta T'$ (calculated using Eqs. 9 and 3); the total energy harvested for each student, and the time taken to perform both the *L*-and *LCS-task*. The maximum average value of $P_L$ was approximately 1.5 mW, corresponding to 2 J of energy harvested in about 22 min of activity, for an average value of $\Delta T'$ of 1.95 K (student three – right leg, *L-task*). Conversely, the calculated minimum value of $P_L$ was approximately 0.5 mW, coinciding to 0.5 J of energy harvested in about 15 min of activity, for an average value of $\Delta T'$ equals to 1.15 K (student one – left leg, *LCS-task*).

In Tables 2 and 3, the letter "L" indicates the left leg and the letter "R" indicates the right leg.

**TABLE 2.** ***L-task*, calculated values for all students.**

| # | Average temp. diff., $\Delta T'$ [K] | | Average power, $P_L$ [mW] | | Total energy harvested, [mJ] | | Time of *task*, [s] |
|---|---|---|---|---|---|---|---|
| | L | R | L | R | L | R | |
| *1* | 1.3±0.3 | 1.3±0.3 | 0.65±0.37 | 0.71±0.40 | 859 | 939 | 1329 |
| *2* | 1.4±0.3 | 1.4±0.3 | 0.78±0.46 | 0.77±0.44 | 1082 | 1063 | 1388 |
| *3* | 1.8±0.3 | 2.0±0.4 | 1.30±0.47 | 1.51±0.58 | 1778 | 2071 | 1369 |
| *4* | 1.3±0.3 | 1.4±0.3 | 0.65±0.37 | 0.83±0.45 | 880 | 1119 | 1351 |

**TABLE 3.** ***LCS-task*, calculated values for all students.**

| # | Average temp. diff., $\Delta T'$ [K] | | Average power, $P_L$ [mW] | | Total energy harvested, [mJ] | | Time of *task*, [s] |
|---|---|---|---|---|---|---|---|
| | L | R | L | R | L | R | |
| *1* | 1.2±0.3 | 1.3±0.3 | 0.53±0.35 | 0.63±0.42 | 448 | 528 | 840 |
| *2* | 1.3±0.3 | 1.3±0.3 | 0.61±0.24 | 0.67±0.30 | 525 | 574 | 862 |
| *3* | 1.4±0.3 | 1.5±0.4 | 0.86±0.43 | 0.86±0.49 | 745 | 748 | 870 |
| *4* | 1.6±0.4 | 1.6±0.4 | 1.07±0.62 | 1.05±0.64 | 854 | 843 | 801 |
| *5* | 1.4±0.4 | 1.4±0.4 | 0.77±0.51 | 0.78±0.49 | 614 | 624 | 797 |
| *6* | 1.3±0.4 | 1.5±0.4 | 0.77±0.54 | 0.84±0.48 | 612 | 666 | 795 |

Since the average values in Tables 2 and 3 were calculated considering the entire duration of tasks, the resulting standard deviation values are large because the activities carried out in the experiments differ between static and motion activities. For instance, the values generated by the F-TEG while the

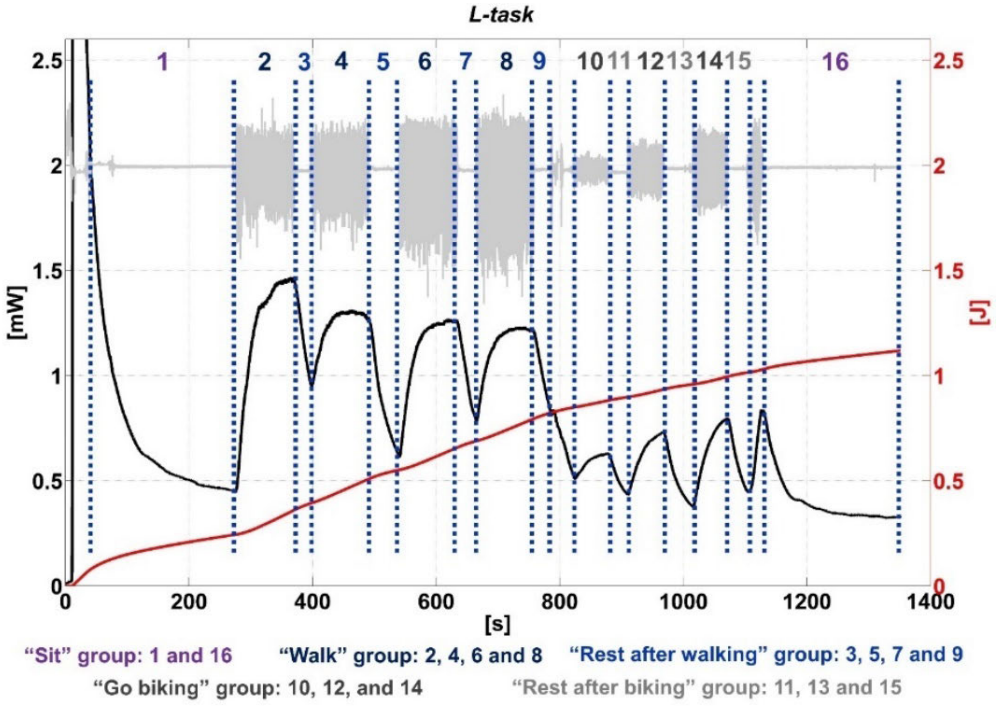


**FIGURE 7.** Pattern of generated F-TEG voltage (black line), accelerometer magnitude (grey line) and total energy harvested (red line) L-task.

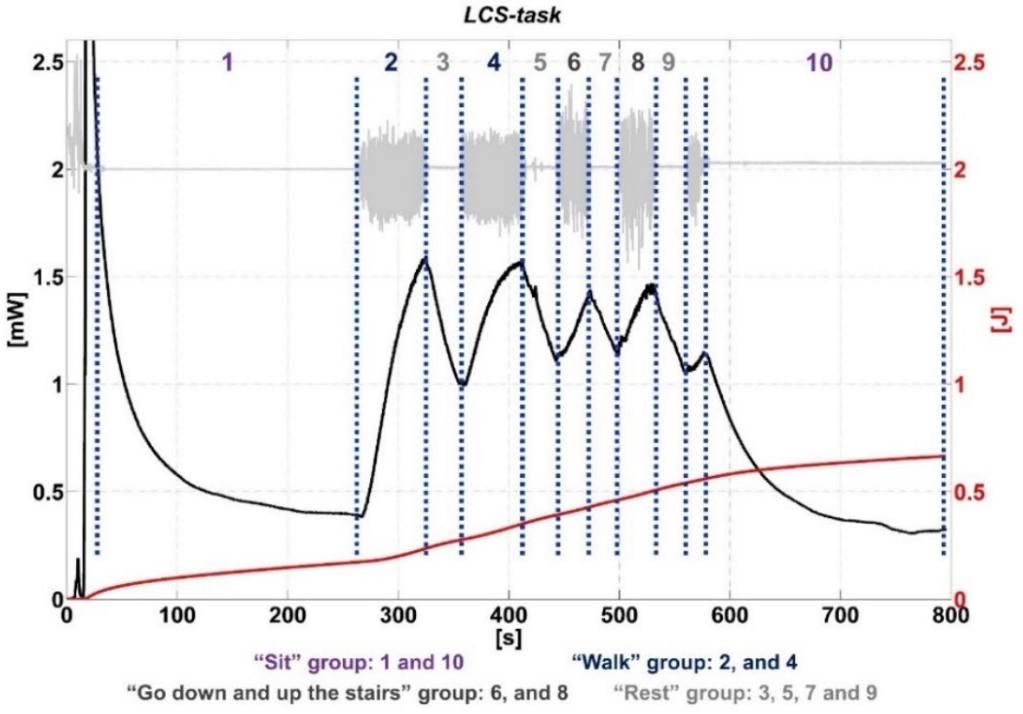


**FIGURE 8.** Pattern of generated F-TEG voltage (black line), accelerometer magnitude (grey line) and total energy harvested (red line) LCS-task.

student is sitting are lower than the values generated by the F-TEG when the same student is walking. To compare average and standard deviation values of a single motor activity carried out by each student, signal segmentation was performed to create the data groups. The dotted blue lines in Figs. 7 and 8 show the points used for signal segmentation,

and the activities that form the data group are labeled with numbers. For the *L-task,* the data groups are: ''Sit'', ''Walk'', ''Rest after walking'', ''Go biking'' and ''Rest after biking''. About the *LCS-task*, the data groups are: ''Sit'', ''Walk'', ''Go down and up the stairs'' and ''Rest'' (see Tables 4S-8S and Tables IXS-XIIS in Supplementary Materials for all results).

For each data group, to graphically compare the multiple pattern signals between them, we use the 'shadedErrorBar' MATLAB® function that computes data over the same period. About the *L-task* groups, the period for ''Sit'' is 210 s; for ''Walk'' is 90 s; for ''Rest after walking'' and ''Rest after biking'' is 15 s, and for ''Go biking'' is 50 s. About the groups of *LCS-task*, the period for ''Sit'' is 180 s; for ''Walk'' is 45 s; for ''Go down and up the stairs'' is 25 s, and for ''Rest'' is 20 s.

Thus, Figs. 9 and 10 show the comparison of average and standard deviation values of the voltage signal, $V_L$, for each data group of both the *L-task* and *LCS- task* (central lines are the mean voltage values and the areas around them represent the standard deviation values).

Fig. 9a shows the signals related to the two activities of the ''Sit'' group; the blue curve represents the beginning, and the black curve is the end of the task. It is clear to note that the blue curve starts from a high value of voltage (95 mV), since it is the exact moment in which the user wears the F-TEG, and then quickly drops to an almost constant value like the value of the black curve: between 35 and 45 mV. Anyhow, the black track shows a larger value of standard deviation than the blue one. This is because the black signals were acquired almost 20 minutes later than the blue ones, and the differences in the voltage values are higher at the end rather than at the beginning of the task.

Fig. 9b shows the signals related to the activities of the ''Walk'' group. Here, the participants were walking with diverse speed, such as slowly, at a preferred walking speed, quickly and following the beat of a metronome set at 120 bpm. As a result, it is easy to note that after 80 s of activity, all mean values converge to a similar value of approximately 60 mV. This means that the frequency of the activity does not affect the value of the voltage generated by the F-TEG. Again, while looking at these signals in the first twenty seconds, the blue curve has a lower mean value than others. This is because the blue curve, which relates to the slow walking, starts after a long period of inactivity, *i.e*. ''Sit'' (∼4 min), rather than the other walking activities that start after ''Rest'' (∼30 s).

Fig. 9c shows signals related to the activities of the ''Go biking'' group. Participants were biking following three rhythms: 60 bpm, 90 bpm and 120 bpm, which were given by a metronome. After 50 s, the mean value of the three curves is approximately 50 mV. Here, the trend of the blue curve, *i.e*. biking at 60 bpm, differs from the others; this is because it starts after a walking activity where the voltage generated by the F-TEG was the highest measured one. Conversely, the mean values of the black and red curves at the beginning of the activity are almost the same because they both start after a biking activity. However, the red curve, *i.e*. biking at 120 bpm, reaches a higher value than the other two because biking in a stationary position at a larger speed generates a higher heat flux exchange in respect to the environment.

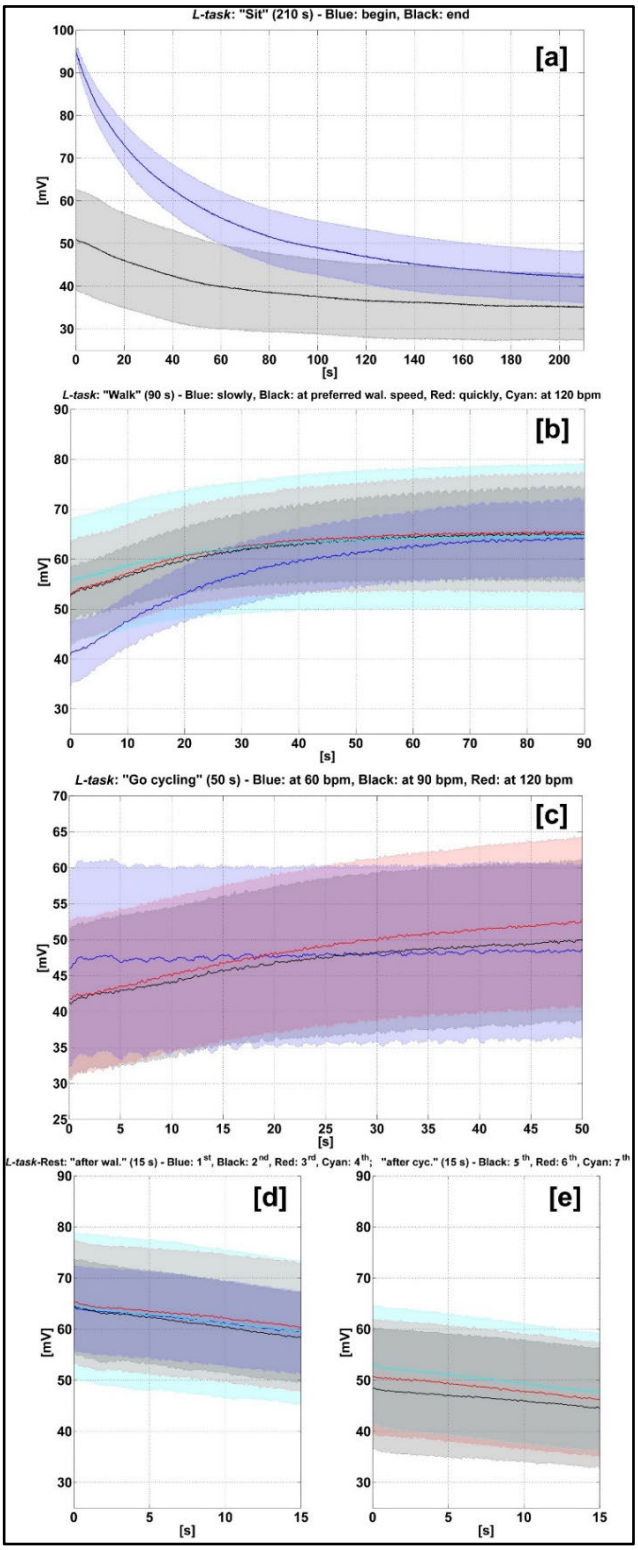


**FIGURE 9.** ***L-task*** **– comparison of voltage signals, $V_L$, generated by the F-TEG during the following activities: "Sit" (a); "Walk" (b); "Go biking" (c); "Rest" (d); "Rest after biking" (e).**

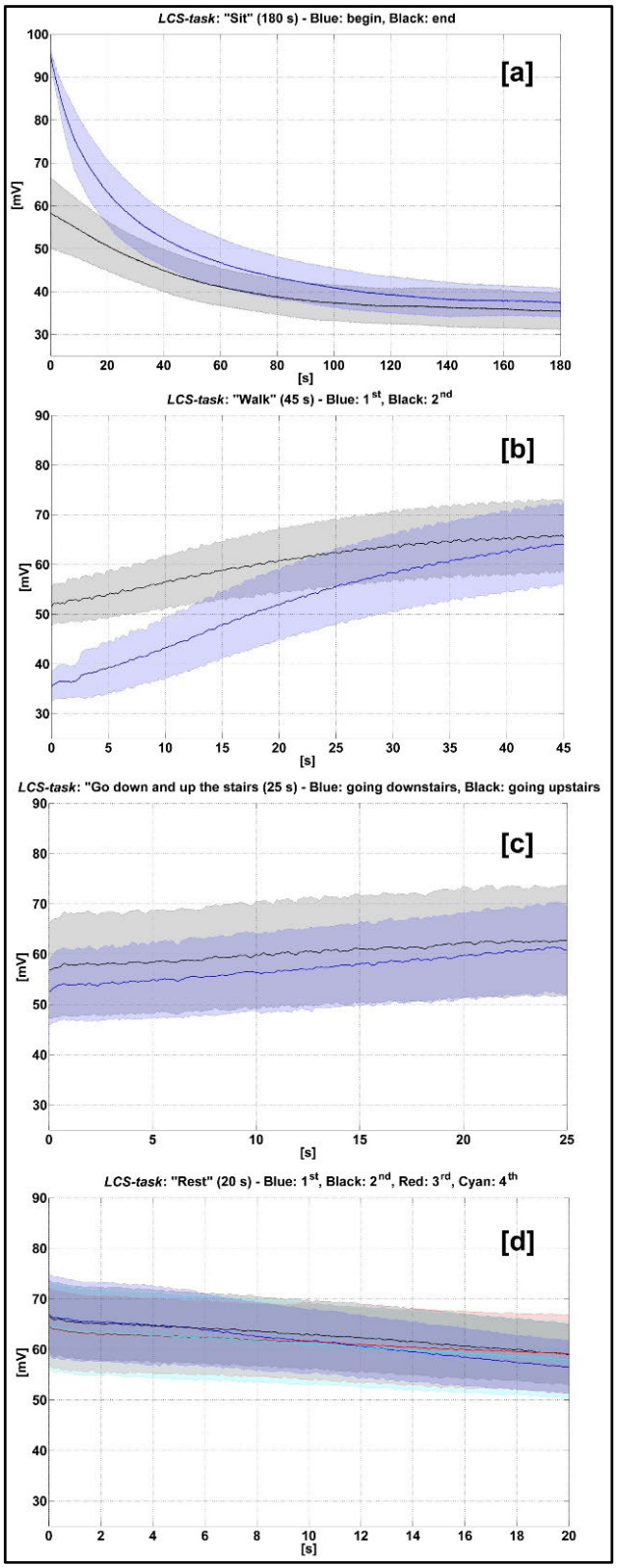


**FIGURE 10.** ***LCS-task*** **– comparison of voltage signals, $V_L$, generated by the F-TEG during the following activities: "Sit" (a); "Walk" (b); "Go down and up the stairs" (c); "Rest" (d).**

Figs. 9d and 9e compare the curve trends of the activities of two ''Rest'' groups: ''Rest after walking'' (Fig. 9d) and ''Rest after biking'' (Fig. 9e). In both graphs, the plotted mean value of voltages decrease by approximately 5 mV; for ''Rest after walking'' from 65 to 60 mV, while for ''Rest after biking'' from 50 to 45 mV. This difference in values depends on the fact that when walking, the F-TEG generates voltage values larger than those generated while users were biking.

Fig. 10a shows the signals related to the activities of the ''Sit'' group. As already observed in Fig. 9a, the mean values of the signals of the blue and black curves of Fig. 10a are almost the same at the end of the activity: in the range between 30 and 40 mV. Again, it is easy to note that the blue curve is the beginning of the task, since its average starting value is 95 mV without any standard deviation. The signals where the standard deviation is not present indicates the exact time when participants wear the F-TEG.

Fig. 10b shows the two curves of the ''Walk'' group: the blue one represents the performance of the former activity, while the black is the latter one. Here, the initial mean value of voltage for the blue curve is lower than the mean value of the black one. It is because the first walking activity was performed after the sitting activity, which lasts for approximately 4 min, while the second walking activity was carried out after resting for approximately 1 min. Anyway, both curves in Fig. 10b end at a mean value of approximately 65 mV.

Fig 10c shows the curves of the activities of the ''Go down and up the stairs'' group. The going downstairs activity is the blue curve while going upstairs is the black one. The mean values of both voltage signals are approximately 60 mV at the end of the activity. However, the black area representing the standard deviation of the signal generated when users were going upstairs is larger than the blue area. It is due to the temperature measured in the stairs being lower than the temperature measured in the corridor, and when participants started to go upstairs, they were on the stairs for a longer time compared to when they started to go downstairs.

Fig. 10d shows the curves related to the activities of the ''Rest'' data group. The blue curve represents the activity of having a rest in the corridor while others are referring to having a rest on the stairs. Indeed, the mean value of the blue signal is the highest at the beginning, but it ends as the lowest. It is due to the temperature in the stairs being lower than the temperature in the corridor, so that the voltage signals measured while participants were having rest in the stairs decreased with a lower slope than the signals measured when the participants were in the corridor. However, the ending mean values for all signals are in the range from 55 to 60 mV after 20 s of activity.

In Figs. 9 and 10, all the measured values for the voltage output, $V_L$, were approximately in the range between 35 to 95 mV. These values correspond to the gradient of temperature across the TCs, $\Delta T'$, between 1.0 and 2.6 °C. However, the thermal contacts at the skin/F-TEG and F-TEG/heatsink interfaces cause a value of $\Delta T'$ to be lower than the gradient of temperature between the two sides of the F-TEG, $\Delta T_{meas}$, which can be easily measured. By simultaneously placing an integrated thermistor probe on the skin and one

between the F-TEG and the heatsink, the value of $\Delta T_{\text{meas}}$ was measured when a user was sitting.

Table 4 shows the obtained result to compare the values of $\Delta T'$ and $\Delta T_{\text{meas}}$.

**TABLE 4.** Values of measured temperature gradient $\Delta T_{\text{meas}}$ and voltage $V_L$ to calculate the value of the ratio $\Delta T_{\text{meas}}/\Delta T'$.

| Measured $\Delta T_{\text{meas}}$, [°C] | Measured $V_L$, [mV] | Calculated E, [mV] | Calculated $\Delta T'$, [°C] | $\frac{\Delta T_{\text{meas}}}{\Delta T'}$ |
|---|---|---|---|---|
| 3.1 | 44.0 | 69.5 | 1.2 | 2.58 |

From the result of Table 4, thermal contacts at the interfaces cause a temperature drop of 2.58 times between the values of $\Delta T_{\text{meas}}$ and $\Delta T'$. Such a result is qualitatively shown in Fig. 11, where the trend of the temperature profile from the body to the environment is explained. As it is clearly visible in Fig. 11, the human tissues act as an excellent heat insulator and most of the temperature drop occurs at the skin/TEG interface because of the large thermal contact resistance, which is due to the rough surface of the skin [39], [40].

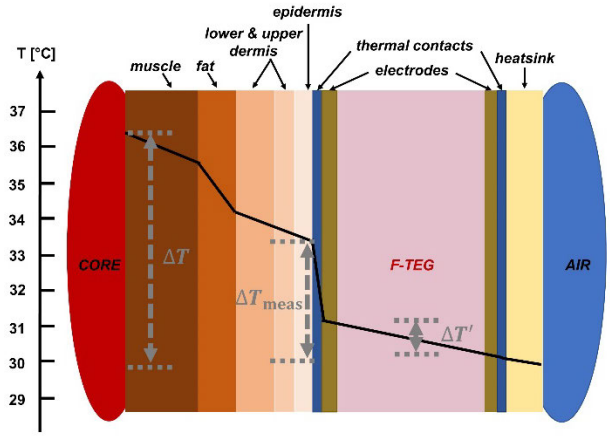


**FIGURE 11.** Temperature profile from the body to the environment.

Moreover, Table 5 and 6 summarize the temperature values measured when participants carried out the *L*- and *LCS-task*, respectively. The measured values refer to the temperatures of the environment and the temperatures of the left and right legs at the beginning and the end of both the tasks.

Regarding the laboratory temperatures for the *L-task*, the values are about the same except for the third participant (*L-task*) where it is 3 degrees lower than the other measured values. For the *LCS-task*, the temperatures measured in the laboratory are higher than those measured in the corridor and stairs; the only exception regards the third participant where the temperature of the corridor is higher than the temperature measured in the laboratory.

While wearing the F-TEG, the value of the leg temperature decreases due to the transfer of the heat flow from the skin surface to the environment. From the values of the leg temperature measured at the beginning and the end of both the tasks, the largest difference is approximately 5 °C for the fifth participant (*LCS-task*), while the smallest is about 2 °C for the fourth participant (*L-task*).

**TABLE 5.** *L-Task*, measured temperatures for all students.

| # | Lab. temp., [°C] | Left (L) leg temp., [°C] | | Right (R) leg temp. [°C] | |
|---|---|---|---|---|---|
| | | Begin | End | Begin | End |
| *1* | 22.6 | 29.4 | 26.0 | 30.2 | 25.8 |
| *2* | 22.1 | 30.2 | 26.3 | 30.2 | 26.1 |
| *3* | 19.0 | 30.4 | 26.2 | 30.8 | 26.1 |
| *4* | 22.5 | 28.7 | 26.3 | 28.7 | 27.0 |

**TABLE 6.** *LCS-Task*, measured temperatures for all students.

| # | Lab. temp., [°C] | Cor. temp., [°C] | Stairs temp., [°C] | Left (L) leg temp., [°C] | | Right (R) leg temp., [°C] | |
|---|---|---|---|---|---|---|---|
| | | | | Begin | End | Begin | End |
| *1* | 23.5 | 22.4 | 21.1 | 28.2 | 26.4 | 28.6 | 26.4 |
| *2* | 23.7 | 22.7 | 21.2 | 30.2 | 26.4 | 30.6 | 26.2 |
| *3* | 21.7 | 22.5 | 21.4 | 29.6 | 26.4 | 29.2 | 26.9 |
| *4* | 25.4 | 22.6 | 21.2 | 31.3 | 27.1 | 30.8 | 27.2 |
| *5* | 23.9 | 22.6 | 21.4 | 30.8 | 25.5 | 30.8 | 25.6 |
| *6* | 25.4 | 21.2 | 20.9 | 30.2 | 26.3 | 31.5 | 26.1 |

To recognize different motor activities, the calculation of the signal gradient was the technique used to separate the stationary and dynamic parts of the F-TEG voltage signal output. A gradient threshold was set to determine insignificant down to zero gradient levels (stationary parts of the signal) and large gradient levels (dynamic parts of the signal). Stationary parts were then defined as the recognized activities, while dynamic parts as the activities not recognized. The threshold value was set to 1% of the gradient maxima for both the *L*- and *LCS-tasks*.

Fig. 12 shows the signals related to the right leg of student four (*L-task*), while Fig. 13 relates to the right leg of student six (*LCS-task*). As is clearly visible for the *L-task*, the recognized activities are much better defined than in the case of the *LCS-task*. This could be due to the time of each performed activity for *LCS-task* being shorter than the time of activities of the *L-task*.

In Supplementary Materials, the F-TEG voltage signals of each student with the corresponding comparison between the activity recognized and not recognised are shown in Figs 5S and 6S.

Fig. 14 shows the result of the experiment where the F-TEG was used as the power source to supply energy for the FXLN8361Q analog accelerometer. The experimental test was carried out in a laboratory of the VSB-Technical University of Ostrava at a temperature of approximately 23.5 °C. While performing the "Go biking" activity at a preferred speed, using an exercise bike, the user was wearing the measurement system on the left leg over the ankle, and the FXLN8361Q analog accelerometer was placed on a desk

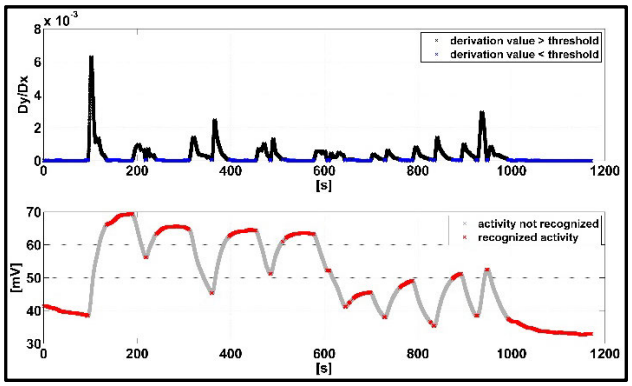


**FIGURE 12.** *L-task* – the top of the picture shows the calculated signal gradient, while the bottom side shows the corresponding recognized activities (red parts of the signal).

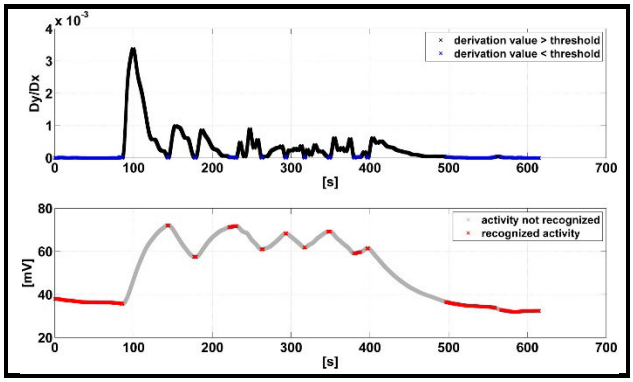


**FIGURE 13.** *LCS-task* – the top of the picture shows the calculated signal gradient, while the bottom side shows the corresponding recognized activities (red parts of the signal).

close to the user. According to the datasheet, the accelerometer output on the $z$-axis for such a placement is 1 g.

As it clearly visible from Fig. 14, when $V_{OUT}$ reached 3.3 V, the voltage stored in the capacitor, $V_{STORE}$, started to increase, getting to 5 V in approximately 350 s. Then, once the switch was closed to supply energy to the load, the resulting operating time for the FXLN8361Q accelerometer was approximately 25 s.

According to the FXLN8361Q datasheet, the voltage output of the accelerometer had to be around 1 V, and the measured output was 1.1 V, thereby confirming its proper functioning. Once the accelerometer was powered on, $V_{STORE}$ started to decrease. The accelerometer turned off when $V_{STORE}$ dropped to approximately 1.5 V. To allow $V_{STORE}$ to recharge the auxiliary capacitor to 5 V, the load should be disconnected from the circuit.

## IV. DISCUSSIONS

Nowadays, wearable devices are increasingly used for remote health monitoring as they represent a technological breakthrough in the diffusion of digital health. However, commercially available wearables do not fully meet the users' needs in terms of battery life.

Harvesting the energy from the body heat dissipated in the environment can be an interesting solution to prolong

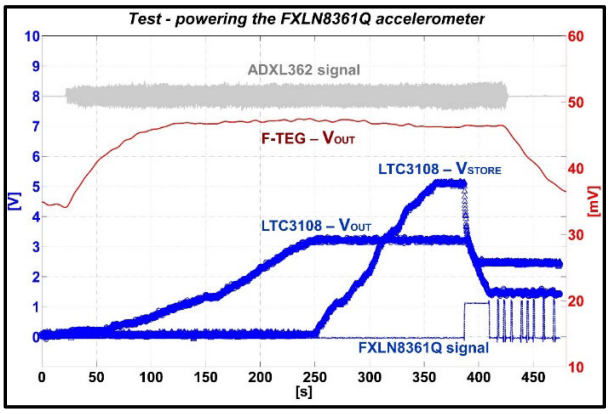


**FIGURE 14.** Result of the experiment where the F-TEG was used as the power source to supply energy for the FXLN8361Q analog accelerometer.

the operating time of wearables. In 1996, Thad Starner was one of the first researchers to investigate the feasibility study to develop a self-powered wearable computing device [19]. In the first decade of 2000s, Vladimir Leonov designed many health-oriented wearable devices powered by TEGs [41]. These devices were bulky, which made them uncomfortable to be worn by humans. Nowadays, the research effort in this field focuses on developing wearable devices based on flexible TEGs, which can easily follow the irregular shape of the skin ensuring the comfort for the end user [24], [42].

In the proposed work, a wearable F-TEG was analyzed in terms of harvesting the body heat energy and to preliminarily understand if it is possible to distinguish between different motor activities from the voltage signal generated by the F-TEG.

Usually, wearable devices are placed on legs to detect motor activities, so the F-TEG equipped with the accelerometer was worn above the ankle.

Students of VSB-Technical University of Ostrava were recruited to carry out two tasks with multiple motor activities: the *L-task* in the laboratory, and the *LCS-task* between the laboratory, the corridor and the stairs of the university.

Regarding the *L-task*, the acquired data were divided into groups such as "Sit", "Walk", "Rest after walk", "Go biking" and "Rest after biking", while for the *LCS-task* the resulting groups were "Sit", "Walk", "Go down and up the stairs" and "Rest".

Since there are redundant groups of activities between the *L-* and *LCS-tasks* and the values of energy harvested by the students do not differ much between them (see the results in Tables 2 and 3), the data discussion concerns the following set of motor activities:

- "Sit" (both *L-* and *LCS-tasks*).
- "Walk" (both *L-* and *LCS-tasks*).
- "Rest" (both *L-* and *LCS-tasks*).
- "Go biking" (only *L-task*).
- "Go down and up the stairs" (only *LCS-tasks*).

Out of ten recruited students, four carried out the *L-tasks* and six the *LCS-tasks*. A total of twenty measurements were

acquired since each student wore the F-TEG on both the left and right leg.

The following Table 7 summarizes the obtained results for the above set of motor activities, in terms of voltage, rate of energy harvesting and power density. It shows the mean values with the standard deviation for all the acquired measurements except for the case of the third student performing the *L-task*. For this case, the laboratory temperature was 19 °C, a value far below the values of the laboratory temperature measured while the other participants were performing the *L-task*, so that it was excluded from the final discussion.

**TABLE 7. Values of temperature gradient, voltage, rate of energy harvesting, power density and F-TEG conversion efficiency.**

| *Activity* | Temp. diff., $\Delta T'$ [°C] | Voltage, $V_L$ [mV] | Rate of energy harvesting, [mJ $s^{-1}$] | Power density, [μW $cm^{-2}$] | $\eta$, $P_L/\dot{Q}$ [%] |
|---|---|---|---|---|---|
| *-Sit* | 1.1±0.1 | 38.2±3.1 | 0.5 ± 0.1 | 8.3±1.3 | 0.05 |
| *-Walk* | 1.5±0.2 | 59.7±6.4 | 1.1 ± 0.2 | 20.3±4.2 | 0.08 |
| *-Rest* | 1.6±0.2 | 57.5±6.3 | 1.0 ± 0.2 | 18.7±4.1 | 0.07 |
| *-Go biking* | 1.2±0.1 | 42.6±2.6 | 0.6 ± 0.1 | 10.2±1.2 | 0.05 |
| *-Rest after biking* | 1.1±0.1 | 39.7±1.4 | 0.6 ± 0.1 | 8.8±0.6 | 0.05 |
| *-Go down & up the stairs* | 1.7±0.2 | 61.0±7.7 | 1.1 ± 0.3 | 21.1±5.2 | 0.08 |

In Table 7, the mean value of the difference of temperature across the TCs varies from 1.1 to 1.7 °C. While users were performing the mentioned activities, the resulting voltage values, generated by the F-TEG, were between 38.2 and 61.0 mV. These values correspond to a rate of energy harvesting between 0.5 and 1.1 mJ $s^{-1}$, and a power density in the range from 8.3 to 21 $\mu$W $cm^{-2}$. The conversion efficiency of the F-TEG, $\eta$, is calculated as the ratio between the electrical power output across the load and the rate of heat dissipated from the body to the F-TEG. As result, the calculated value of $\eta$ is between 0.05% and 0.08%.

In comparison with the current scientific literature for which flexible thermoelectric generators are used for harvesting the thermal energy on the body, the chosen F-TEG is one of the most powerful devices. Indeed, by considering the steady state of the ''Sit'' activity, the F-TEG generated 38.2 mV, and from Eq. (12) the corresponding power across the load is approximately 440 $\mu$W. Such a value is comparable to the result obtained by Nozariasbmarz, *et al.*, in which a TEG-based armband generated 340 $\mu$W of electrical power to turn on an LED [39]. Under steady state conditions, Kim *et al.* used the F-TEG for harvesting the body heat on the forearm by generating a power density of 13 $\mu$W $cm^{-2}$ [25]. This value is larger than the value obtained in our study (8.3 $\mu$W $cm^{-2}$) because the skin temperature on the leg is lower than that on the forearm.

The value of power density obtained for the ''Rest'' activity is larger than the value of the ''Sit'' activity because it was always after a ''Walk'' activity, and it had a much shorter duration than ''Sit''. Therefore, we cannot state that the ''Rest'' activity was carried out under a steady state condition. The same consideration is true for the ''Rest after biking'' activity. Here, the values are low (8.8 $\mu$W $cm^{-2}$) because the results obtained for the ''Go biking'' activity are low too: 10.2 $\mu$W $cm^{-2}$.

The highest values generated by the F-TEG are for the ''Walk'' and ''Go down & up the stairs'' activities; the voltage is 60 mV, the rate of energy harvesting 1.0 mJ $s^{-1}$, and the power density 20 $\mu$W $cm^{-2}$, approximately.

The increase of the values generated by the F-TEG when users were moving is due to an increased convective heat transfer at the cold side of the F-TEG.

In the steady state position, the human body is subjected to natural air convection, thus the main variable to determine the rate of energy harvesting is the temperature gradient across the two sides of the F-TEG. Conversely, while users are in motion, the speed of the air with respect to the person generates a forced air convection, resulting in a further variable that significantly affects the performance of the F-TEG.

The measurements of skin temperature at the beginning and the end of the experiments indicate that the heat transfer lowers the skin temperature *via* convection. Such a result can be interpreted in two different ways. Regarding the former, the lowering of the temperature can cause a cold sensation resulting in user discomfort. Regarding the latter, the F-TEG can be used as a skin refrigerator for body thermoregulation, which in some cases is a benefit for the humans [43]. Thus, the F-TEG can be used not only to harvest the body heat energy but also as a sensor to detect temperature and convective heat flux variations [44].

An innovation regarding the use of the F-TEG can be the correlation between the pattern of the signal output with the recognition of diverse human motor activities. As is shown in Figs. 12 and 13, the semi-stationary parts of the F-TEG signal are recognized after a certain period of performing an activity or when there is a significative change in the slope of the curve. Our analysis shows that if the F-TEG amplitude signal keeps an almost constant value, the activity performed by the user is continuative and it does not change over time. Again, in Figs. 12 and 13, the presence of single red dots shows a variation in the signal direction, which means that the motor activity changed at that precise instant. Indeed, the single red dots are always followed by periods where the activity is not recognized because the amplitude of the F-TEG signal significantly varies over the time.

About testing the F-TEG as a direct power source to supply energy to the FXLN8361Q accelerometer, the result shows that the sensor was operating for only 25 s. This is due to the power consumption value of the FXLN8361Q accelerometer, which is approximately 500 $\mu$W.

The use of the F-TEG as an on-body energy harvester for designing a self-powered system is only reasonable if the load consumes less than 10 $\mu$W.

## V. CONCLUSION

In this work, a commercial F-TEG worn on the lower leg, above the ankle, was used to harvest the body heat energy while users were carrying out different motor activities in the form of ''Sit'', ''Walk'', ''Rest'', ''Go biking'', ''Rest after biking'', and ''Go down and up the stairs''. The maximum measured value of power density was 20.3 $\mu$W cm$^{-2}$ for the ''Walk'' activity, corresponding to a gradient of temperature between the hot and cold side of the TCs constituting the F-TEG of 1.5 °C, while the minimum measured value of power density was 8.3 $\mu$W cm$^{-2}$ for the ''Sit'' activity, corresponding to a gradient of temperature of 1.1 °C.

The F-TEG was also used to try to power an analog accelerometer, which consumes 500 $\mu$W. As a result, the analog accelerometer was operating for only 25 s, hence indicating that the electrical load should consume much less for the design of a wearable system powered solely by energy generated by the F-TEG. Conversely, the use of the F-TEG is highly advised to be used as a supplementary power source to increase the operating time of wearables.

Regarding the analysis of the signal pattern generated by the F-TEG to distinguish diverse motor activities, the mathematical model of signal gradient was adopted. As a preliminary result, the recognition of an activity can be traced back to the semi-stationary parts of the signal. Conversely, the non-stationary part of the signal indicates the occurrence of a change with respect to an activity carried out previously. It is a preliminary result that must be deepened through the execution of several continuous activities without any rest periods.

In future work, machine learning techniques will be applied and analyzed for the recognition of the different motor activities.

## REFERENCES

[1] P. Bonato, ''Wearable sensors/systems and their impact on biomedical engineering,'' *IEEE Eng. Med. Biol. Mag.*, vol. 22, no. 3, pp. 18–20, May 2003, doi: 10.1109/MEMB.2003.1213622.

[2] A. Pantelopoulos and N. G. Bourbakis, ''A survey on wearable sensor-based systems for health monitoring and prognosis,'' *IEEE Trans. Syst., Man, Cybern. C, Appl. Rev.*, vol. 40, no. 1, pp. 1–12, Jan. 2010, doi: 10.1109/TSMCC.2009.2032660.

[3] C. Caramia, D. Torricelli, M. Schmid, A. Munoz-Gonzalez, J. Gonzalez-Vargas, F. Grandas, and J. L. Pons, ''IMU-based classification of Parkinson's disease from gait: A sensitivity analysis on sensor location and feature selection,'' *IEEE J. Biomed. Health Informat.*, vol. 22, no. 6, pp. 1765–1774, Nov. 2018, doi: 10.1109/JBHI.2018.2865218.

[4] D. Bryant, J. Boyd, J. Harris, M. Smith, S. Garcia-Vergara, Y.-P. Chen, and A. Howard, ''An infant smart-mobile system to encourage kicking movements in infants at-risk of cerebral palsy,'' in *Proc. IEEE Workshop Adv. Robot. Social Impacts (ARSO)*, Mar. 2017, pp. 1–5, doi: 10.1109/ARSO.2017.8025187.

[5] J. Montes, D. Zanotto, S. Dunaway Young, R. Salazar, D. C. De Vivo, and S. Agrawal, ''Gait assessment with solesound instrumented footwear in spinal muscular atrophy,'' *Muscle Nerve*, vol. 56, no. 2, pp. 230–236, Aug. 2017, doi: 10.1002/mus.25484.

[6] R. Finkel, E. Bertini, F. Muntoni, and E. Mercuri, ''209th ENMC international workshop: Outcome measures and clinical trial readiness in spinal muscular atrophy 7–9 november 2014, Heemskerk, The Netherlands,'' *Neuromuscular Disorders*, vol. 25, no. 7, pp. 593–602, Jul. 2015, doi: 10.1016/j.nmd.2015.04.009.

[7] A. Godfrey, V. Hetherington, H. Shum, P. Bonato, N. H. Lovell, and S. Stuart, ''From A to Z: Wearable technology explained,'' *Maturitas*, vol. 113, pp. 40–47, Jul. 2018, doi: 10.1016/j.maturitas.2018.04.012.

[8] A. Cadei, A. Dionisi, E. Sardini, and M. Serpelloni, ''Kinetic and thermal energy harvesters for implantable medical devices and biomedical autonomous sensors,'' *Meas. Sci. Technol.*, vol. 25, no. 1, Jan. 2014, Art. no. 012003, doi: 10.1088/0957-0233/25/1/012003.

[9] A. Proto, M. Penhaker, S. Conforto, and M. Schmid, ''Nanogenerators for human body energy harvesting,'' *Trends Biotechnol.*, vol. 35, no. 7, pp. 610–624, Jul. 2017, doi: 10.1016/j.tibtech.2017.04.005.

[10] R. J. M. Vullers, R. van Schaijk, I. Doms, C. Van Hoof, and R. Mertens, ''Micropower energy harvesting,'' *Solid-State Electron.*, vol. 53, no. 7, pp. 684–693, Jul. 2009, doi: 10.1016/j.sse.2008.12.011.

[11] A. W. Van Herwaarden and P. M. Sarro, ''Thermal sensors based on the Seebeck effect,'' *Sens. Actuators A, Phys.*, vol. 10, nos. 3–4, pp. 321–346, Nov. 1986, doi: 10.1016/0250-6874(86)80053-1.

[12] D. Champier, ''Thermoelectric generators: A review of applications,'' *Energy Convers. Manage.*, vol. 140, pp. 167–181, May 2017, doi: 10.1016/j.enconman.2017.02.070.

[13] S. Qing, A. Rezaniakolaei, L. A. Rosendahl, and X. Gou, ''An analytical model for performance optimization of thermoelectric generator with temperature dependent materials,'' *IEEE Access*, vol. 6, pp. 60852–60861, 2018, doi: 10.1109/ACCESS.2018.2874947.

[14] N. Jaziri, A. Boughamoura, J. Müller, B. Mezghani, F. Tounsi, and M. Ismail, ''A comprehensive review of thermoelectric generators: Technologies and common applications,'' *Energy Rep.*, vol. 6, pp. 264–287, Dec. 2020, doi: 10.1016/j.egyr.2019.12.011.

[15] X. Li, C. Xie, S. Quan, Y. Shi, and Z. Tang, ''Optimization of thermoelectric Modules' number and distribution pattern in an automotive exhaust thermoelectric generator,'' *IEEE Access*, vol. 7, pp. 72143–72157, 2019, doi: 10.1109/ACCESS.2019.2919689.

[16] K. Xie, S. Wu, C. Yang, Y. Ruan, and Y. Hong, ''A new seafloor hydrothermal power generation device based on waterproof thermoelectric modules,'' *IEEE Access*, vol. 8, pp. 70762–70772, 2020, doi: 10.1109/ACCESS.2020.2986857.

[17] M. Markiewicz, P. Dziurdzia, T. Konieczny, M. Skomorowski, L. Kowalczyk, T. Skotnicki, and P. Urard, ''Software controlled low cost thermoelectric energy harvester for ultra-low power wireless sensor nodes,'' *IEEE Access*, vol. 8, pp. 38920–38930, 2020, doi: 10.1109/ACCESS.2020.2975424.

[18] J. Lee, D. Kim, H. Sul, and S. H. Ko, ''Thermo-Haptic materials and devices for wearable virtual and augmented reality,'' *Adv. Funct. Mater.*, to be published, doi: 10.1002/adfm.202007376.

[19] T. Starner, ''Human-powered wearable computing,'' *IBM Syst. J.*, vol. 35, no. 3.4, pp. 618–629, 1996, doi: 10.1147/sj.353.0618.

[20] Y. Yang and J. Liu, ''Evaluation of the power-generation capacity of wearable thermoelectric power generator,'' *Frontiers Energy Power Eng. China*, vol. 4, no. 3, pp. 346–357, Sep. 2010, doi: 10.1007/s11708-010-0112-z.

[21] G. J. Snyder and E. S. Toberer, ''Complex thermoelectric materials,'' *Nature Mater.*, vol. 7, no. 2, pp. 105–114, Feb. 2008, doi: 10.1038/nmat2090.

[22] S. J. Kim, H. E. Lee, H. Choi, Y. Kim, J. H. We, J. S. Shin, K. J. Lee, and B. J. Cho, ''High-performance flexible thermoelectric power generator using laser multiscanning lift-off process,'' *ACS Nano*, vol. 10, no. 12, pp. 10851–10857, Dec. 2016, doi: 10.1021/acsnano.6b05004.

[23] S. J. Kim, H. Choi, Y. Kim, J. H. We, J. S. Shin, H. E. Lee, M.-W. Oh, K. J. Lee, and B. J. Cho, ''Post ionized defect engineering of the screen-printed bi 2 te 2.7 se 0.3 thick film for high performance flexible thermoelectric generator,'' *Nano Energy*, vol. 31, pp. 258–263, Jan. 2017, doi: 10.1016/j.nanoen.2016.11.034.

[24] C. S. Kim, G. S. Lee, H. Choi, Y. J. Kim, H. M. Yang, S. H. Lim, S.-G. Lee, and B. J. Cho, ''Structural design of a flexible thermoelectric power generator for wearable applications,'' *Appl. Energy*, vol. 214, pp. 131–138, Mar. 2018, doi: 10.1016/j.apenergy.2018.01.074.

[25] C. S. Kim, H. M. Yang, J. Lee, G. S. Lee, H. Choi, Y. J. Kim, S. H. Lim, S. H. Cho, and B. J. Cho, ''Self-powered wearable electrocardiography using a wearable thermoelectric power generator,'' *ACS Energy Lett.*, vol. 3, no. 3, pp. 501–507, Mar. 2018, doi: 10.1021/acsenergylett.7b01237.

[26] B. J. Cho, S. J. Kim, J. S. Shin, S. Yim, H. D. Choi, Y. Kim, C. S. Kim, and J. H. We, ''Flexible thermoelectric element and production method therefor,'' U.S. Patent 2018 0 233 648 A1, Aug. 16, 2018.

[27] J. Olivo, S. Carrara, and G. De Micheli, ''Energy harvesting and remote powering for implantable biosensors,'' *IEEE Sensors J.*, vol. 11, no. 7, pp. 1573–1586, Jul. 2011, doi: 10.1109/JSEN.2010.2085042.

[28] F. Suarez, A. Nozariasbmarz, D. Vashaee, and M. C. Özturk, ''Designing thermoelectric generators for self-powered wearable electronics,'' *Energy Environ. Sci.*, vol. 9, no. 6, pp. 2099–2113, 2016, doi: 10.1039/c6ee00456c.

[29] G. Min, T. Singh, J. Garcia-Canadas, and R. Ellor, "Evaluation of thermoelectric generators by I–V curves," *J. Electron. Mater.*, vol. 45, no. 3, pp. 1700–1704, Mar. 2016, doi: 10.1007/s11664-015-4180-z.
[30] A. Proto, L. Peter, M. Augustynek, M. Cerny, and M. Penhaker, "Flexible TEG on the ankle for measuring the power generated while performing activities of daily living," *Lék. Tech.*, vol. 48, no. 3, pp. 84–90, 2018.
[31] D. Trojaniello, A. Cereatti, E. Pelosin, L. Avanzino, A. Mirelman, J. M. Hausdorff, and U. D. Croce, "Estimation of step-by-step spatio-temporal parameters of normal and impaired gait using shank-mounted magneto-inertial sensors: Application to elderly, hemiparetic, parkinsonian and choreic gait," *J. NeuroEng. Rehabil.*, vol. 11, no. 1, p. 152, 2014, doi: 10.1186/1743-0003-11-152.
[32] F. A. Storm, C. J. Buckley, and C. Mazzà, "Gait event detection in laboratory and real life settings: Accuracy of ankle and waist sensor based methods," *Gait Posture*, vol. 50, pp. 42–46, Oct. 2016, doi: 10.1016/j.gaitpost.2016.08.012.
[33] A. Proto, D. Bibbo, M. Cerny, D. Vala, V. Kasik, L. Peter, S. Conforto, M. Schmid, and M. Penhaker, "Thermal energy harvesting on the bodily surfaces of arms and legs through a wearable thermo-electric generator," *Sensors*, vol. 18, no. 6, p. 1927, Jun. 2018, doi: 10.3390/s18061927.
[34] A. Proto, J. Jargus, L. Peter, J. Vondrak, M. Schmidt, and M. Penhaker, "Encapsulation of mTEGs for on-body energy harvesting," in *Proc. Joint Int. EUROSOI Workshop Int. Conf. Ultimate Integr. Silicon (EUROSOI-ULIS)*, Apr. 2019, pp. 1–4, doi: 10.1109/EUROSOI-ULIS45800.2019.9041861.
[35] J. Vondrak, M. Schmidt, A. Proto, M. Penhaker, J. Jargus, and L. Peter, "Using miniature thermoelectric generators for wearable energy harvesting," in *Proc. 4th Int. Conf. Smart Sustain. Technol. (SpliTech)*, Jun. 2019, pp. 1–6, doi: 10.23919/SpliTech.2019.8782997.
[36] W. Velasquez, M. S. Alvarez-Alvarado, and J. Salvachua, "Body mass index in human walking on different types of soil using graph theory," *IEEE Access*, vol. 6, pp. 47935–47942, 2018, doi: 10.1109/ACCESS.2018.2866557.
[37] D. M. Savastano, A. M. Gorbach, H. S. Eden, S. M. Brady, J. C. Reynolds, and J. A. Yanovski, "Adiposity and human regional body temperature," *Amer. J. Clin. Nutrition*, vol. 90, no. 5, pp. 1124–1131, Nov. 2009, doi: 10.3945/ajcn.2009.27567.
[38] *BMI Ranges*. Accessed: Jan. 27, 2021. [Online]. Available: https://www.nhs.uk/common-health-questions/lifestyle/what-is-the-body-mass-index-bmi/
[39] A. Nozariasbmarz, F. Suarez, J. H. Dycus, M. J. Cabral, J. M. LeBeau, M. C. Öztürk, and D. Vashaee, "Thermoelectric generators for wearable body heat harvesting: Material and device concurrent optimization," *Nano Energy*, vol. 67, Jan. 2020, Art. no. 104265, doi: 10.1016/j.nanoen.2019.104265.
[40] D. Lee, H. Park, G. Park, J. Kim, H. Kim, H. Cho, S. Han, and W. Kim, "Liquid-metal-electrode-based compact, flexible, and high-power thermoelectric device," *Energy*, vol. 188, Dec. 2019, Art. no. 116019, doi: 10.1016/j.energy.2019.116019.
[41] V. Leonov, "Thermoelectric energy harvesting of human body heat for wearable sensors," *IEEE Sensors J.*, vol. 13, no. 6, pp. 2284–2291, Jun. 2013, doi: 10.1109/JSEN.2013.2252526.
[42] Y. Sargolzaeiaval, V. P. Ramesh, T. V. Neumann, V. Misra, D. Vashaee, M. D. Dickey, and M. C. Öztürk, "Flexible thermoelectric generators for body heat harvesting—Enhanced device performance using high thermal conductivity elastomer encapsulation on liquid metal interconnects," *Appl. Energy*, vol. 262, Mar. 2020, Art. no. 114370, doi: 10.1016/j.apenergy.2019.114370.
[43] S. Hong, Y. Gu, J. K. Seo, J. Wang, P. Liu, Y. S. Meng, S. Xu, and R. Chen, "Wearable thermoelectrics for personalized thermoregulation," *Sci. Adv.*, vol. 5, no. 5, May 2019, Art. no. eaaw0536, doi: 10.1126/sciadv.aaw0536.
[44] J. Yuan, R. Zhu, and G. Li, "Self-powered electronic skin with multisensory functions based on thermoelectric conversion," *Adv. Mater. Technol.*, vol. 5, no. 9, Jul. 2020, Art. no. 2000419, doi: 10.1002/admt.202000419.

**ANTONINO PROTO** was born in Milan, Italy, in 1987. He received the M.Sc. degree in biomedical engineering from the Campus Bio-Medico University of Rome, in 2013, and the Ph.D. degree in applied electronics from the University of Roma Tre, in 2017. He is currently a Postdoctoral Researcher with the Department of Cybernetics and Biomedical Engineering, Technical University of Ostrava. His research interests include human body energy harvesting, wireless energy transfer, and low-power electronics for biomedical applications.

**JAROSLAV VONDRAK** was born in Ostrava, Czechia, in 1994. He received the M.Sc. degree in biomedical engineering from the Technical University of Ostrava, in 2018, where he is currently pursuing the Ph.D. degree with the Department of Cybernetics and Biomedical Engineering. His research interests include biomedical signal processing, applied mathematics in biomedicine, and the research field of human body energy harvesting.

**MARTIN SCHMIDT** was born in Sumperk, Czechia, in 1994. He received the M.Sc. degree in biomedical engineering from the Technical University of Ostrava, in 2018, where he is currently pursuing the Ph.D. degree with the Department of Cybernetics and Biomedical Engineering. His research interests include human body energy harvesting and the development of electronic hardware for biomedical systems.

**JAN KUBICEK** was born in Ostrava, Czechia. He received the M.Sc. degree in biomedical engineering and the Ph.D. degree in technical cybernetics from the Technical University of Ostrava, in 2012 and 2018, respectively. He is currently an Assistant Professor with the Department of Cybernetics and Biomedical Engineering, Technical University of Ostrava. His research interests include applied image and signal processing in medicine and statistical analysis of biomedical data.

**OJAN MAJIDZADEH GORJANI** was born in Tehran, Iran, in 1990. He received the M.Sc. degree in electrical engineering from the Wroclaw University of Science and Technology, in 2018. He is currently pursuing the Ph.D. degree with the Department of Cybernetics and Biomedical Engineering, Technical University of Ostrava. His research interests include artificial intelligence, big data analysis, and smart homes automation.

**JAN HAVLIK** received the M.Sc. degree in electronics and the Ph.D. degree in electrical engineering theory from Czech Technical University in Prague, in 2001 and 2008, respectively. He is currently an Assistant Professor with the Department of Circuit Theory, Czech Technical University, Prague. His research interests include medical electronics, hardware development for biomedical systems, biomedical signal processing, and telemedicine and telemonitoring.

**MAREK PENHAKER** received the M.Sc. degree in measurement and control and the Ph.D. degree in technical cybernetics from the Technical University of Ostrava, in 1996 and 2000, respectively. Since 2018, he has been a Full Professor of biomedical engineering. He is currently the Principal Investigator of the Biomedical Engineering Group, Department of Cybernetics and Biomedical Engineering, Technical University of Ostrava. His research interests include electronics for medical devices, biomedical signal processing, and home telemetry.